Origin of Second-Harmonic Signals in Octave Bandwidth Traveling-Wave Tubes

Patrick Y. Wong, Y. Y. Lau, *Fellow, IEEE*, David Chernin, Brad W. Hoff, *Member, IEEE*, and Ronald M. Gilgenbach, *Life Fellow, IEEE*

***Abstract*— In a helix traveling-wave tube (TWT) with a bandwidth exceeding one octave, the second harmonic of an input signal near the low end of the band will experience exponential growth. In such a case, we have found that the nonlinear electron orbits in the beam, as opposed to the orbital bunching exhibited in the linear electron orbits, are the main source for second-harmonic generation. This unexpected result is due to the synchronous amplification of the second harmonic. We demonstrate this phenomenon from the solution of the nonlinear equations that we have formulated that govern evolution of the second-harmonic field; these equations may include axial variations of the Pierce parameters. In several test cases, we compare the theory with simulation using the CHRISTINE large signal TWT code. Good agreement between theory and simulation is found.**

***Index Terms*— Frequency multiplier, harmonic generation, traveling-wave tube (TWT).**

I. Introduction

A HELIX traveling-wave tube (TWT) with octave bandwidth necessarily employs a circuit with low dispersion over the full operating band. This means that the phase velocity of a signal near the low end of the band and that of its second harmonic at the upper end of the band will be nearly the same. If the electron beam has a similar drift velocity as this phase velocity, the electrons can synchronously interact with the circuit wave over a wide range of frequencies. An input signal near the low frequency end of the amplification band may then generate a second-harmonic signal if the beam current carries a second-harmonic component, which could be due to some nonlinearity in the orbits. This paper analyzes the generation of second harmonic in a TWT, due solely to an input signal at the (fundamental) frequency, ω_0, in the case that the second-harmonic experiences finite small-signal gain. We focus on the physical mechanism by which the second harmonic is generated, its analytic description, and its validation with a simulation code.

A well-known nonlinear process in vacuum electronics that leads to harmonic beam current due to an input signal of a single frequency ω_0 is crowding of the electron orbits [1], in which neighboring electrons are getting closer together. This occurs in the drift tube of a klystron and the harmonic content in the ac current has been calculated exactly in a 1-D model [1], [2]; this calculation has been explicitly shown to be valid even for the case where the electron orbits have crossed, i.e., when charge overtaking has occurred [2]. Significant harmonic current appears even if the electron velocity is strictly in the linear regime, that is, the velocity of an electron has only a dc component, plus a fundamental frequency component at a very low level [1], [3], [4]. The nonlinearity in the ac current arises kinematically, from the exact solution to the nonlinear continuity equation that accounts for orbital crowding (including charge overtaking) in the linearized electron orbits. While this orbital crowding process has been well known for a klystron in generating harmonic ac current, it was explicitly evaluated for a TWT only recently [5]. The second-harmonic ac current in the beam in a TWT was found to be quite high, reaching 1/4 of the dc beam current, even though the electron's ac velocity is in the linear regime (as in the klystron analysis). This level of second-harmonic current in a TWT, due to orbital crowding, was corroborated by the code, CHRISTINE [6].

Despite the high harmonic current due to orbital crowding that was described in the preceding paragraph, in this paper, we report another nonlinear effect that is far more important in the generation of second-harmonic power in a wideband TWT. The latter is due to the nonlinear correction in the electron orbit, which is described by the nonlinear convective derivative in the force law, $v_1(\partial v_1/\partial z)$, where $v_1 = v_{10}e^{j\omega_0 t - jk_0 z}$ is the linearized electron fluid velocity at the fundamental frequency, whose wavenumber $k_0 \approx (\omega_0/v_0)$ where v_0 is the dc beam velocity. This convective derivative, $v_1(\partial v_1/\partial z)$, then contributes a "force" proportional to $v_{10}^2 e^{j2\omega_0 t - j2k_0 z}$ (analogous to the "ponderomotive force" in the latter's derivation [7]). This "force" is a traveling wave at the second-harmonic

Manuscript received October 6, 2017; revised December 7, 2017; accepted December 15, 2017. Date of publication January 5, 2018; date of current version January 22, 2018. This work was supported in part by the Air Force Office of Scientific Research under Award FA9550-15-1-0097 and Award FA9550-14-1-0309, in part by the Air Force Research Laboratory under Award FA9451-14-1-0374, in part by the Office of Naval Research under Award N00014-16-1-2353, and in part by L3 Technologies. The review of this paper was arranged by Editor L. Kumar. *(Corresponding author: Y. Y. Lau.)*

P. Y. Wong, Y. Y. Lau, and R. M. Gilgenbach are with the Department of Nuclear Engineering and Radiological Sciences, University of Michigan, Ann Arbor, MI 48109 USA (e-mail: pywong@umich.edu; yylau@umich.edu; rongilg@umich.edu).

D. Chernin is with Leidos Corporation, Reston, VA 20190 USA (e-mail: david.p.chernin@leidos.com).

B. W. Hoff is with the Air Force Research Laboratory, Kirtland Air Force Base, Albuquerque, NM 87117 USA (e-mail: brad.hoff@us.af.mil).

Color versions of one or more of the figures in this paper are available online at http://ieeexplore.ieee.org.

Digital Object Identifier 10.1109/TED.2017.2785284

frequency. It has a phase velocity also synchronized with the electron beam because $(\omega/k) = (2\omega_0/2k_0) = (\omega_0/k_0) \approx v_0$. This "force" may then synchronously excite a second-harmonic wave, both in time and space, which makes it a much more powerful contributor to second-harmonic generation. The ac harmonic current due to orbital crowding, described in the preceding paragraph, does not possess this property of synchronization in both time and space, and is therefore a much weaker contributor in the generation of RF power at the second harmonic. This is a rather unexpected finding, because we did not anticipate that the nonlinear term $v_1(\partial v_1/\partial z)$ would be so important, as v_1 is admittedly in the linear regime. Comparison with CHRISTINE simulation confirmed these facts, as we shall show in Section III.

We should mention that largely based on Nordsieck's seminal paper [8] on the nonlinear TWT theory, harmonic generation in broadband TWT was extensively studied [9]–[12]. These works did not identify the physical origin of the harmonic generation, even though they have all included the effect of orbital crowding (including charge overtaking). It is also not immediately clear how these works could be applied to a realistic tube that has a spatially nonuniform circuit loss, and a sever region. The analytic approach, based on a straightforward expansion given in this paper, is a marked departure from the Nordsieck formulation [8]. It readily includes spatially nonuniform circuit loss and a sever, in addition to the discovery that orbital crowding (including charge overtaking) is not the dominant cause for harmonic generation. The numerical examples presented below validated our approach, whose results were favorably compared with the nonlinear simulation code, CHRISTINE [6]. Other works on harmonic generation in a TWT may be referenced, which used either an Eulerian [13], [14] or Lagrangian description [15]. None of these prior works recognized the main theme of this paper, namely, the dominant influence of synchronous excitation, over orbital crowding, in harmonic generation in a wideband TWT.

The present theory was motivated by the current experiments on harmonic generation in a bifrequency recirculating planar magnetron [16]. There are also contemporary simulations and experiments of harmonic generation in a TWT [17]. This paper might provide a new theoretical framework for such works.

In Section II, we extend the classical TWT theory of Pierce [18] to include the generation of second harmonic. We shall indicate how the nonsynchronous charge overtaking effect, and the synchronous excitation due to $v_1(\partial v_1/\partial z)$, would enter in our formulation of harmonic generation. Numerical examples for a TWT with a sever and spatially nonuniform cold-tube loss are given in Section III, and compared with simulation results. Section IV presents the conclusion.

II. Formulation

We shall use the Eulerian description to formulate the force law and the circuit equation. We shall indicate how harmonic current due to orbital crowding can be accounted for in such a formulation. We shall closely follow, but extend Pierce's classical three-wave theory of TWTs [1], [18] to include harmonic generation. The lowest order (linear) theory is identical to Pierce's theory. We separately consider the force law (electronic equation) and the circuit equation.

We digress to remark that we shall use Pierce's classical three-wave theory of TWT, instead of the more complete Pierce's four-wave theory ([1], p. 361), for the following reasons.

1) We shall compare our analytic formulation with the CHRISTINE code, which is a well-validated large signal helix TWT simulation code. The governing equations solved by CHRISTINE reduce to those of Pierce's three-wave theory for small-signal amplitudes.
2) Our careful case study of a dielectric TWT [19] shows that the value of the space-charge parameter, QC, would be different between the three-wave and four-wave theories.
3) Perhaps most importantly, since the four-wave theory includes the reverse-propagating circuit mode, an absolute instability could arise if the beam current is sufficiently high [20], [21], and such a possibility is beyond the scope of this paper. Pierce's three-wave theory of TWT rules out the excitation of absolute instability.

A. Electronic Equation

We assume that the electron beam is cold, confined by an infinite axial magnetic field, and drifts at constant velocity v_0 in the unperturbed (dc) state. In the 1-D model, the nonlinear force law for the electron fluid reads

$$\left(\frac{\partial}{\partial t} + v(z,t)\frac{\partial}{\partial z}\right) v(z,t) = -\frac{e}{m_e} E(z,t) \tag{1}$$

where the fluid velocity $v(z,t)$ is related to the fluid displacement $s(z,t)$ by

$$v(z,t) = \left(\frac{\partial}{\partial t} + v(z,t)\frac{\partial}{\partial z}\right) s(z,t) \tag{2}$$

and the total electric field $E(z,t)$ consists of circuit and space-charge electric fields

$$E(z,t) = E_C(z,t) + E_{SC}(z,t). \tag{3}$$

The circuit field E_C is excited by the ac current, as modeled by Pierce, and the space-charge field E_{SC} will also be modeled by Pierce through his space-charge parameter, QC [1], [18]. Note that all quantities in (1)–(3) are expressed in the Eulerian description.

We expand the dependent variables $\{s, v, E\}$ as follows:

$$s(z,t) = s_0 + \varepsilon s_1(z,t) + \varepsilon^2 s_2(z,t) + \cdots \tag{4a}$$

$$v(z,t) = v_0 + \varepsilon v_1(z,t) + \varepsilon^2 v_2(z,t) + \cdots \tag{4b}$$

$$E(z,t) = E_0 + \varepsilon E_1(z,t) + \varepsilon^2 E_2(z,t) + \cdots \tag{4c}$$

where ε is a small expansion parameter in harmonics, which measures the ratio of the beam's perturbation velocity to its dc velocity. We substitute (4a)–(4c) into (1) and (2) and collect

terms of the same order in ε. The ε^0 terms describe the dc state. The ε^1 terms describe the familiar linearized force law

$$\left(\frac{\partial}{\partial t}+v_0\frac{\partial}{\partial z}\right)v_1=-\frac{e}{m_e}E_1 \tag{5}$$

$$v_1=\left(\frac{\partial}{\partial t}+v_0\frac{\partial}{\partial z}\right)s_1. \tag{6}$$

The ε^2 terms give

$$\left(\frac{\partial}{\partial t}+v_0\frac{\partial}{\partial z}\right)v_2=-\frac{e}{m_e}E_2-v_1\frac{\partial v_1}{\partial z} \tag{7}$$

$$v_2=\left(\frac{\partial}{\partial t}+v_0\frac{\partial}{\partial z}\right)s_2+v_1\frac{\partial s_1}{\partial z} \tag{8}$$

which describe the generation of second harmonic on account of the $v_1(\partial v_1/\partial z)$ in the right-hand member of (7). If the ε^1 terms give the linearized response to the fundamental frequency ω_0, we may write the ε^n terms as

$$\{s_n, v_n, E_n\}=\{s_n(z), v_n(z), E_n(z)\}e^{j(n\omega_0)t}. \tag{9}$$

Thus, the operator $(\partial/\partial t)$ in (5) and (6) may be replaced by $j\omega_0$ for v_1 and s_1, whereas the operator $(\partial/\partial t)$ in (7) and (8) may be replaced by $j2\omega_0$ for v_2 and s_2. Equations (5)–(8) then become first-order ordinary differential equations in z.

We next follow Pierce [1], [18] and decompose the total electric field E into the circuit and space-charge electric fields, for the nth harmonic fields:

$$E_n=E_{nC}+E_{n\mathrm{SC}}=E_{nC}+\frac{4(n\omega_0)^2Q_nC_n^3s_n}{e/m_e}. \tag{10}$$

The last equality in (10), giving the explicit form of the space-charge electric field, follows Pierce's definition of the QC parameter (as applied to a wave at the nth harmonic frequency, $\omega=n\omega_0$). In Pierce's notation, the electronic equation at the fundamental frequency ($n=1$) reads [1], [5], [18]

$$\left[\left(\frac{d}{dz}+j\frac{\omega_0}{v_0}\right)^2+4\left(\frac{\omega_0}{v_0}\right)^2Q_1C_1^3\right]s_1(z)=-\frac{e}{m_ev_0^2}E_{1C}(z). \tag{11}$$

The electronic equation at the second harmonic ($n=2$) reads

$$\left[\left(\frac{d}{dz}+j\frac{2\omega_0}{v_0}\right)^2+4\left(\frac{2\omega_0}{v_0}\right)^2Q_2C_2^3\right]s_2(z)$$
$$=-\frac{e}{m_ev_0^2}E_{2C}(z)-\frac{v_1(z)}{v_0^2}\frac{dv_1(z)}{dz}$$
$$-\left(\frac{d}{dz}+j\frac{2\omega_0}{v_0}\right)\frac{v_1(z)}{v_0}\frac{ds_1(z)}{dz}. \tag{12}$$

It is clear that the linear theory for the fundamental frequency (11) is identical to Pierce's theory. Equation (12) then is an extension to Pierce's theory for the second harmonic. Note that (12) is similar in form to (11), except for the additional nonlinear forcing terms at the end of the RHS of (12). These nonlinear terms, comprised of quantities from the fundamental, are what generate and drive the evolution of the second harmonic.

The excitation of the circuit electric field E_{nC} also follows the classical TWT theory and is considered next.

B. Circuit Equation

The excitation of the circuit wave electric field E_{1C} at the fundamental frequency ($n=1$) is the same as the classical, the linear theory of TWTs. In Pierce's notation, it reads[1]

$$\left(\frac{d}{dz}+j\frac{\omega_0}{v_0}[1+(b_1-jd_1)C_1]\right)E_{1C}(z)=j\frac{m_e}{ev_0}\omega_0^3C_1^3s_1(z). \tag{13}$$

Note that the RHS of (13) represents the ac current at the fundamental frequency, which is proportional to the electronic displacement at the fundamental frequency, s_1. It is this ac current, at the fundamental frequency that excites the circuit field, E_{1C}. The Pierce three-wave dispersion relation may readily be obtained from (11) and (13) by assuming a wave-like solution for $s_1(z)$, $E_1(z)\propto e^{-j\beta z}$ [22].

The ac current at the second-harmonic frequency would similarly excite the circuit wave electric field at the second harmonic, E_{2C}. The composite electronic displacement, s_1 and s_2, now both contribute to the second-harmonic current, kinematically. The displacement s_2, at the second-harmonic frequency, will contribute to a second-harmonic current that is represented by the first term in the RHS of the circuit equation, now constructed for the second harmonic

$$\left(\frac{d}{dz}+j\frac{2\omega_0}{v_0}[1+(b_2-jd_2)C_2]\right)E_{2C}(z)$$
$$=j\frac{m_e}{ev_0}(2\omega_0)^3C_2^3s_2(z)+j\frac{m_e}{ev_0}\Lambda I_2(s_1) \tag{14}$$

which may readily be compared with (13). The last term in (14) represents the second-harmonic current due solely to the displacement s_1. It is denoted by $I_2(s_1)$, and its physical origin comes from orbital crowding from the first-order (linearized) electron orbit, s_1. Dong *et al.* [5] provided the procedure to compute the spatial evolution of $I_2(s_1)$, which is also valid even if charge overtaking occurs. Λ here is a coupling coefficient that is defined as: $\Lambda\equiv -j(((2\omega_0)^2v_0)/I_0)C_2^3$. It turns out that nonlinear contributions to the s_2 term [that are described by the last two terms in the RHS of (12)] in the RHS of (14) are much more important than the $I_2(s_1)$ term.

Equations (11) and (13) may be solved for the evolution of the fundamental frequency solutions, $s_1(z)$ and $E_{1C}(z)$, subject to the boundary conditions at $z=0$ (TWT input)

$$s_1(z=0)=0 \tag{15a}$$

$$\left.\frac{\partial s_1}{\partial z}\right|_{z=0}=0 \tag{15b}$$

$$E_{1C}(z=0)=E_{10} \tag{15c}$$

where E_{10} is the circuit electric field at the input, which is at the fundamental frequency. Equation (15b) states that there is no velocity perturbation at the input, as can be seen from $v_1=j\omega_0s_1+v_0(\partial s_1/\partial z)$ and using (15a). Once $s_1(z)$ and $v_1(z)$

[1]A more careful expansion would show that (13) should read

$$\left(\frac{d}{dz}+j\frac{\omega_0}{v_0}[1+(b_1-jd_1)C_1]\right)E_{1C}(z)=j\frac{m_e}{ev_0}\omega_0^3C_1^3(1+C_1b_1)^2s_1(z). \tag{13a}$$

Equation (13a) was used in CHRISTINE and will be used in the comparison. For ease of exposition, we will continue to use (13).

TABLE I
TABULATION OF PARAMETERS FOR TEST CASES

Parameter	Value
Input power (P_{in})	1 mW
Length of circuit (L)	9.5758 cm
Beam radius (R_b)	0.05 cm
Beam voltage (V_b)	3 kV
Beam current (I_0)	0.170 A

Frequency [GHz]	v_{ph}/c	K [Ω]	b	C	QC
4.5	0.103818	111.27	0.337	0.116	0.281
9.0	0.093908	8.97	2.961	0.050	1.053

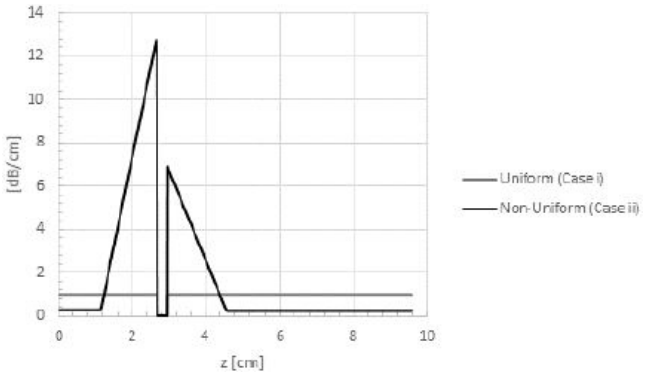

Fig. 1. Attenuation profile of a helix TWT used for the test cases. The mid-stream sever of radius $R_{\text{sever}} = 0.2794$ cm is located between $z = 2.667$ cm and $z = 2.921$ cm.

are obtained, (12) and (14) may be solved for the evolution of the second-harmonic solutions, $s_2(z)$ and $E_{2C}(z)$, subject to the boundary conditions at $z = 0$

$$s_2(z=0) = 0 \tag{16a}$$

$$\left.\frac{\partial s_2}{\partial z}\right|_{z=0} = 0 \tag{16b}$$

$$E_{2C}(z=0) = 0. \tag{16c}$$

Equations (16c) and (15c) state that all second-harmonic quantities are generated by the input signal at the fundamental frequency. Note further that the second-harmonic signal that is generated will have a definite phase relation with respect to the input signal.

III. NUMERICAL EXAMPLES

We shall consider several test cases involving a helix TWT with parameters tabulated in Table I. This example includes a sever and spatially nonuniform cold-tube loss. In Table I, v_{ph} is the wave phase velocity (normalized to the speed of light in vacuum, c), K, b, C, and QC are the Pierce interaction impedance, detuning parameter, gain parameter, and ac "space-charge" parameter, respectively. For the Pierce circuit cold-tube loss parameter d [1], [22], we consider the cases of: 1)

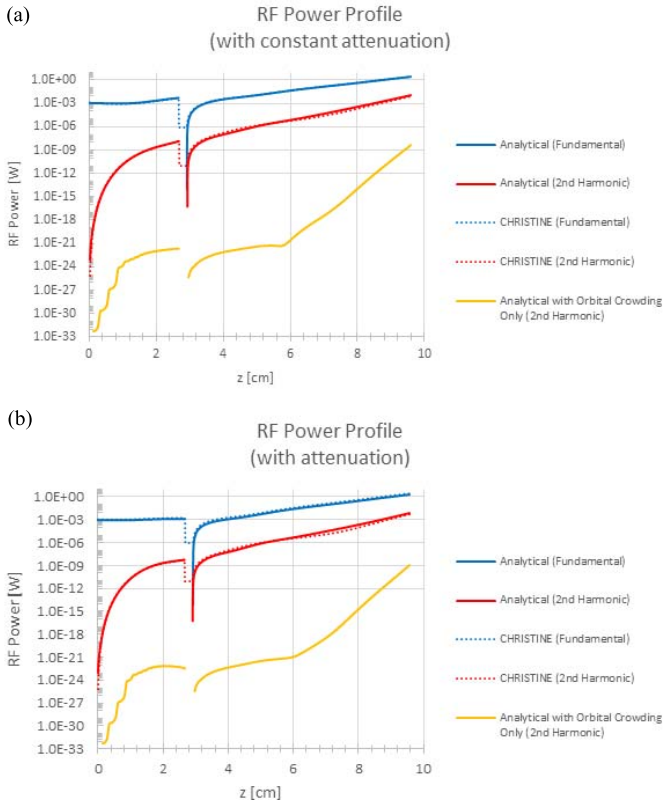

Fig. 2. RF power profile in semi-log plot for (a) case with constant attenuation and (b) the case with the attenuation profile. The bottom curves show second-harmonic RF power due only to the orbital crowding term, $\Lambda I_2(s_1)$, in (14).

a spatially uniform profile (d = constant) given by the gray line and 2) an attenuation profile given by the black line, as shown in Fig. 1.

As can be seen from Fig. 1, there is an addition of a sever midstream. The modeling of the sever region is given in the Appendix.

The results for the RF power profile for both test cases (uniform and nonuniform attenuation profiles) described are shown in Fig. 2. The top four curves in Fig. 2(a) and (b) show the RF power profile for both test cases and for both the fundamental and second harmonic in semilog plot. There is excellent agreement between the analytical calculation (blue solid curves) and the CHRISTINE code (blue dashed curves) for the evolution of the fundamental, as is expected. For the second harmonic, it may be seen that there is also reasonable agreement. This may be more explicitly seen in the linear plots of the second-harmonic RF power profile (Fig. 3).

As can be seen from Fig. 3, there is reasonable agreement between the analytic theory (red solid curves) and CHRISTINE (red dashed curves) for the second-harmonic RF power profile. In the presever region, [Fig. 3(a) and (c)], there is excellent agreement for both constant attenuation and spatial taper (attenuation profile). In the postsever region, [Fig. 3(b) and (d)], the analytic formulation differs from CHRISTINE by only 50%, after the second-harmonic RF power exponentiates by six orders of magnitude beyond the sever region. This difference might well be attributed to the

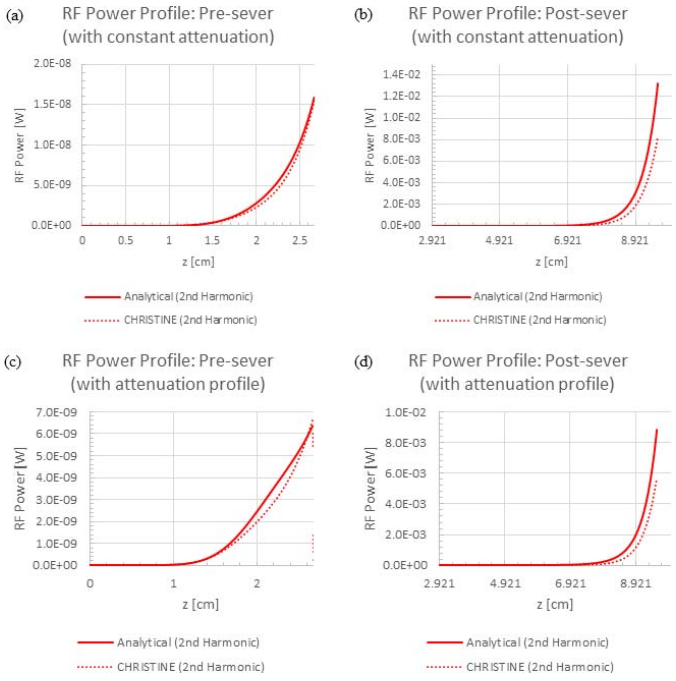

Fig. 3. RF power profile for the second harmonic in linear plot for (a) and (b) case with constant attenuation and (c) and (d) case with the attenuation profile.

differences in modeling the sever region in CHRISTINE and in the analytic theory (Appendix). These tests may then be taken as a validation of both the CHISTINE code and the analytic theory, for both the fundamental and second harmonic, with and without the effects of spatial tapers.

It should be noted that the synchronous nonlinear terms in s_2 [i.e., the $v_1(\partial v_1/\partial z)$ and $v_1(\partial s_1/\partial z)$ terms in (12)] are the main contributors to describing the growth of the second-harmonic RF power. Without these nonlinear terms for s_2, but retaining only the orbital crowding term $\Lambda I_2(s_1)$ in the RHS of (14), the second-harmonic RF power is orders of magnitude lower, as shown in the bottom curve in Fig. 2(a) and (b). The nonsynchronicity of the orbital crowding term means that the second-harmonic RF power does not grow beyond its initial value (0 W). In other words, the top four curves in Fig. 2(a) and (b), and all curves in Fig. 3, are hardly changed if we drop the $\Lambda I_2(s_1)$ term in the RHS of (14), when we solve (12) and (14). It should also be noted that from no initial power at the second-harmonic frequency and an input power of 1 mW at the fundamental frequency, RF power on the order of 10 mW is derived at the second harmonic for this example.

IV. Conclusion

In a helix TWT that has an octave bandwidth (or greater), the second harmonic of the input signal at the fundamental frequency may be within the tube's amplification band and thus may also be amplified. In such a case, there are two possible sources of harmonic content: the process of orbital crowding (similar to that in klystrons) and nonlinearities in the electron orbits. Much to our surprise, it was found that orbital crowding did not play as important of a role as was initially thought. Rather, specific nonlinear terms in the governing equation for the electron beam played a much more important role in describing the RF power growth. The synchronicity of these terms and thus of the second-harmonic field to the beam provided the mechanism for this growth. That is, it was found $(2\omega_0/2k_0) \approx v_0$ at the second harmonic, the condition for amplification in a TWT.

In this paper, we have provided a method to ascertain the synchronous nonlinear terms in the governing equations for the beam–circuit interaction. In so doing, we have provided an extension to Pierce's original formulation to describe harmonics in the electron beam. The method in this paper also recovers Pierce's original equations for the beam–circuit interaction at the fundamental (input) frequency and allows for axial variations in the Pierce parameters.

To test whether or not our analytical method is viable, several test cases were considered with comparisons made with the large-signal, nonlinear CHRISTINE simulation code. In these test cases, a helix TWT with a midstream sever and an attenuation profile was considered. As was expected, excellent agreement in the RF power profiles was found between theory and CHRISTINE at the fundamental. We have also validated the second-harmonic RF power profile in the pre and postsever regions for the cases of uniform and nonuniform attenuation.

Future work may include extension to higher harmonics, and application of this theory to harmonic generation in other devices.

Appendix

We model the midstream sever ($z_- < z < z_+$, $z_- = 2.667$ cm, $z_+ = 2.921$ cm, see Fig. 1) in the test cases as a cylindrical drift tube that is perfectly conducting. We assume that the circuit electric field is completely cut off in the sever region (i.e., $E_C = 0$). Information from the presever region to the postsever region is transmitted completely through the beam. The governing equation for the evolution of the beam within the sever region is

$$\left(\frac{\partial}{\partial t} + v_0\frac{\partial}{\partial z}\right) v(z,t) + \omega_q^2 s(z,t) = 0, \quad z_- < z < z_+. \tag{A1}$$

Assuming $e^{j(n\omega_0)t}$ dependence for a signal of frequency $\omega = n\omega_0$, (A1) becomes

$$\left(jn\omega_0 + v_0\frac{d}{dz}\right) v_n(z) + \omega_{qn}^2 s_n(z) = 0. \tag{A2}$$

Equation (A1) is just a statement of the (linearized) force law with space-charge effects and no circuit fields [3]. Here, $\omega_q = \omega_p F$ is the reduced plasma frequency, where the plasma frequency reduction factor F was calculated using the method prescribed in [23] (in particular, the case where the pencil electron beam is concentric with a metallic cylinder). The initial conditions for (A2) are $s_n(z)$ and $v_n(z)$ are continuous at $z = z_-$.

At the exit of the sever region ($z = z_+$), $s_n(z)$ and $v_n(z)$ are continuous. In addition, $E_C(z_+) = 0$, meaning that the circuit field is zero at $z = z_+$. These are the boundary conditions for the postsever region ($z > z_+$) for (11) and (13) for $n = 1$, and for (12) and (14) for $n = 2$.

REFERENCES

[1] G. W. Gewartowski and H. A. Watson, *Principles of Electron Tubes*. Princeton, NJ, USA: Van Nostrand, 1966.

[2] C. B. Wilsen, Y. Y. Lau, D. P. Chernin, and R. M. Gilgenbach, "A note on current modulation from nonlinear electron orbits," *IEEE Trans. Plasma Sci.*, vol. 30, no. 3, pp. 1176–1178, Jun. 2002, doi: 10.1109/TPS.2002.801571.

[3] Y. Y. Lau, D. P. Chernin, C. Wilsen, and R. M. Gilgenbach, "Theory of intermodulation in a klystron," *IEEE Trans. Plasma Sci.*, vol. 28, no. 3, pp. 959–970, Jun. 2000.

[4] M. Friedman, J. Krall, Y. Y. Lau, and V. Serlin, "Externally modulated intense relativistic electron beams," *J. Appl. Phys.*, vol. 64, no. 7, pp. 3353–3379, Oct. 1988.

[5] C. F. Dong *et al.*, "Harmonic content in the beam current in a traveling-wave tube," *IEEE Trans. Electron Devices*, vol. 62, no. 12, pp. 4285–4292, Dec. 2015, doi: 10.1109/TED.2015.2490584.

[6] T. M. Antonsen, Jr., and B. Levush, "CHRISTINE: A multifrequency parametric simulation code for traveling wave tube amplifiers," NRL, Sydney, NSW, Australia, Tech. Rep. NRL/FR/6840-97-9845, Apr. 1997.

[7] D. R. Nicholson, *Introduction to Plasma Theory*. New York, NY, USA: Wiley, 1983, p. 31.

[8] A. Nordsieck, "Theory of the large signal behavior of traveling-wave amplifiers," *Proc. IRE*, vol. 41, no. 5, pp. 630–637, May 1953.

[9] P. K. Tien, L. R. Walker, and V. M. Wolontis, "A large signal theory of traveling wave amplifiers," *Proc. IRE*, vol. 35, no. 2, pp. 260–277, Mar. 1955.

[10] J. E. Rowe, "A large-signal analysis of the traveling-wave amplifier: Theory and general results," *IRE Trans.-Electron Devices*, vol. 3, no. 1, pp. 39–56, Jan. 1956.

[11] A. J. Giarola, "A theoretical description for the multiple-signal operation of a TWT," *IEEE Trans. Electron Devices*, vol. ED-15, no. 6, pp. 381–395, Jun. 1968.

[12] N. J. Dionne, "Harmonic generation in octave bandwidth traveling-wave tubes," *IEEE Trans. Electron Devices*, vol. ED-17, no. 4, pp. 365–372, Apr. 1970.

[13] S. K. Datta, P. K. Jain, M. D. R. Narayan, and B. N. Basu, "Nonlinear Eulerian hydrodynamical analysis of helix traveling-wave tubes," *IEEE Trans. Electron Devices*, vol. 45, no. 9, pp. 2055–2062, Sep. 1998.

[14] J. G. Wohlbier, J. H. Booske, and I. Dobson, "The multifrequency spectral Eulerian (MUSE) model of a traveling wave tube," *IEEE Trans. Plasma Sci.*, vol. 30, no. 3, pp. 1063–1075, Jun. 2002, doi: 10.1109/TPS.2002.801603.

[15] Y. V. Gulyaev, V. F. Kravchenko, and A. A. Kuraev, "Vavilov–Cherenkov amplifiers with irregular electrodynamic structures," *Phys.-Uspekhi*, vol. 47, no. 6, pp. 583–599, Jun. 2004, doi: 10.1070/PU2004v047n06ABEH001748.

[16] G. B. Greening, N. M. Jordan, S. C. Exelby, D. H. Simon, Y. Y. Lau, and R. M. Gilgenbach, "Multi-frequency recirculating planar magnetrons," *Appl. Phys. Lett.*, vol. 109, no. 7, p. 074101, Aug. 2016, doi: 10.1063/1.4961070.

[17] X. Meng, Y. Gong, T. Tang, H. Gong, and G. Travish, "The research of 140 GHz high harmonic traveling wave tube," in *Proc. IEEE Int. Vac. Electron. Conf. (IVEC)*, Apr. 2016, pp. 1–2. [Online]. Available: http://doi.org/10.1109/IVEC.2016.7561832

[18] J. R. Pierce, *Traveling Wave Tubes*. New York, NY, USA: Van Nostrand, 1950.

[19] D. H. Simon *et al.*, "On the evaluation of Pierce parameters C and Q in a traveling wave tube," *Phys. Plasmas*, vol. 24, no. 3, p. 033114, 2017, doi: 10.1063/1.4978474.

[20] D. M. H. Hung *et al.*, "Absolute instability near the band edge of traveling-wave amplifiers," *Phys. Rev. Lett.*, vol. 115, no. 12, p. 124801, 2015, doi: 10.1103/PhysRevLett.115.124801.

[21] A. P. Kuznetsov, S. P. Kuznetsov, A. G. Rozhnev, E. V. Blokhina, and L. V. Bulgakova, "Wave theory of a traveling-wave tube operated near the cutoff," *Radiophys. Quantum Electron.*, vol. 47, no. 5, pp. 356–373, 2004.

[22] I. M. Rittersdorf, T. M. Antonsen, Jr., D. Chernin, and Y. Y. Lau, "Effects of random circuit fabrication errors on the mean and standard deviation of small signal gain and phase of a traveling wave tube," *IEEE J. Electron Devices Soc.*, vol. 1, no. 5, pp. 117–128, May 2013, doi: 10.1109/JEDS.2013.2273794.

[23] G. M. Branch and T. G. Mihran, "Plasma frequency reduction factors in electron beams," *IRE Trans.-Electron Devices*, vol. 2, no. 2, pp. 3–11, Apr. 1955.

Patrick Y. Wong, photographs and biographies not available at the time of publication.

Y. Y. Lau (M'98–SM'06–F'08) received the B.S., M.S., and Ph.D. degrees in electrical engineering from the Massachusetts Institute of Technology, Cambridge, MA, USA.

He is currently a Professor with the University of Michigan, Ann Arbor, MI, USA, specialized in RF sources, heating, and discharge.

Prof. Lau received the IEEE Plasma Science and Applications Award and the John R. Pierce Award for Excellence in Vacuum Electronics. He is an APS Fellow.

David Chernin received the Ph.D. degree in applied mathematics from Harvard University, Cambridge, MA, USA, in 1976.

He has been with Leidos Corporation, Reston, VA, USA, and its predecessor company Science Applications International Corporation, since 1984, where he has conducted research on beam-wave interactions and other topics in the physics of particle accelerators and vacuum electron devices.

Dr. Chernin is a member of the American Physical Society.

Brad W. Hoff (S'04–M'10) received the Ph.D. degree in nuclear engineering from the University of Michigan, Ann Arbor, MI, USA, in 2009.

He is currently a Senior Research Physicist with the Directed Energy Directorate, Air Force Research Laboratory, Kirtland Air Force Base, Albuquerque, NM, USA. His current research interests include high-power microwave sources and applications of additive manufacturing to directed energy technology.

Ronald M. Gilgenbach (S'73–M'74–SM'92–F'06–LF'15) received the B.S. and M.S. degrees from the University of Wisconsin, Madison, WI, USA, in 1972 and 1973, respectively, and the Ph.D. degree from Columbia University, New York, NY, USA, in 1978.

He is currently the Department Chair and the Collegiate Professor with the University of Michigan, Ann Arbor, MI, USA.

Dr. Gilgenbach is a fellow of the APS DPP.